Behavior of ACRBP-deficient mouse sperm
in the female reproductive tract

（ ACRBP KOマウス精子の雌性生殖器内における挙動解析）

2018

筑波大学グローバル教育院

School of the Integrative and Global Majors in University of Tsukuba

Ph.D. Program in Human Biology

Kiyoshi Nagashima (永島 聖)

Contents

Behavior of ACRBP-deficient mouse sperm

in the female reproductive tract

ABBREVIATION

ACR   : acrosin

ACRBP   : proacrosin-binding protein

ADAM3   : a disintegrin and metallopeptidase domain 3

AR   : acrosome reaction

BSA   : bovine serum albumin

CASA   : computer-assisted semen analysis

CBB   : coomassie brilliant blue

DMSO   : dimethyl sulfoxide

GFP   : green fluorescent protein

HYAL5   : hyaluronoglucosaminidase 5

IZUMO1   : Izumo sperm-egg fusion protein 1

LIN   : linearity

mRNA   : messenger RNA

OCC   : oocyte-cumulus complex

PBS   : phosphate-buffered saline

PCR   : polymerase chain reaction

PNA   : peanut agglutinin

PRSS21   : protease, serine 21

RFP   : red fluorescent protein

SPAM1   : sperm adhesion molecule 1

STR   : straightness

TYH   : Toyoda-Yokoyama-Hoshi medium

UTJ   : uterotubal junction

VAP   : average path velocity

VCL   : curvilinear velocity

VSL   : straight-line velocity

WOB   : wobble

ZP   : zona pellucida

ZPBP1   : zona pellucida-binding protein 1

ZPBP2   : zona pellucida-binding protein 2

SUMMARY

Depletion of proacrosin-binding protein, ACRBP/sp32, in mouse sperm exhibits continuous variation in head morphology. Although ACRBP-null male mice show a severely reduced fertility, migration of the mutant sperm in the female reproductive tract remains unknown. In this study, I examined the cause of subfertility in ACRBP-null mice based on observations of sperm behavior in vivo and in vitro. Heterogeneous distributions of morphology and motility in ACRBP-null sperm were shifted to a population carrying similar characteristics to that of wild-type sperm after migration from the uterus to the oviduct through the uterotubal junction. A significantly reduced number of ACRBP-null sperm was found in the oviductal ampulla. The mutant sperm were barely present around the oocytes and accumulated within the cumulus matrix. Interestingly, dispersal of cumulus cells by ACRBP-null sperm was also delayed. These results suggest that the subfertility of ACRBP-null male mice is caused by the reduced sperm number in the oviduct and the defects of sperm penetration through the cumulus.

INTRODUCTION

Mammalian sperm migrate through the female reproductive tract to accomplish fertilization. Ejaculated sperm from male reproductive tract ascend the vagina, cervix, uterus, uterotubal junction (UTJ), and oviductal isthmus and finally reach to the oviductal ampulla where fertilization takes place (Fig. 1). Although more than million mouse sperm are present in the uterus, small number of sperm are selected to migrate through the UTJ connecting the uterus and oviduct. After migrating through the UTJ, the oviductal isthmus temporally stores the ascending sperm and provides physiological changes for sperm to render an ability to fertilize with oocytes, called capacitation (Bedford and Breed, 1994; DeMott et al., 1992; Overstreet et al., 1979; Suarez et al., 2008; Yanagimachi et al., 1994). A process of sperm capacitation includes HCO_3^--induced activation of adenyl cyclase and elevation of cAMP, cholesterol efflux from the sperm membrane, and an increase in protein tyrosine phosphorylation (Coy et al., 2012). Following capacitation, sperm acquire hyperactivation motility through detachment from epithelial cells in the isthmus and swim toward the oviductal ampulla (Chang and Suarez, 2012; Suarez and Pacey, 2006). Sperm encounter the oocyte-cumulus complex (OCC), pass through the cumulus matrix, and penetrate the zona pellucida (ZP) to fuse with the oocyte (Ikawa et al., 2010). Recently, to elucidate processes of sperm migration after entering into the UTJ, transgenic mice expressing fluorescent proteins GFP and RFP in sperm acrosome and midpiece, respectively, have been generated (Hasuwa et al., 2010). The transgenic mice enable us to observe behavior of sperm in the oviduct, including status of the acrosome reaction. The acrosome reaction of sperm, which is a
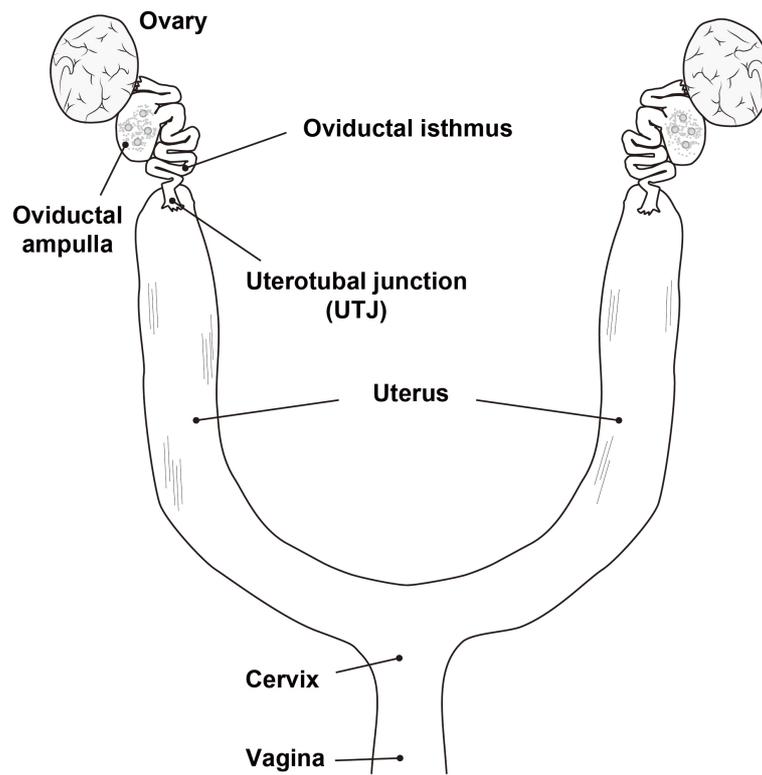
Figure 1. Mouse female reproductive tract
Ejaculated sperm migrate through vagina, cervix, uterus, uterotubal junction (UTJ), and then enter to the oviduct. Oocytes ovulated from the ovary are present in the oviductal ampulla where fertilization takes place.

fusion event between outer acrosomal and plasma membranes, is initiated at the middle region of the oviduct (Spina et al., 2016; Muro et al., 2016). Sperm transport between the isthmus and middle region of oviduct is assisted by shuttling flows produced by myosalpinx contractions (Ishikawa et al., 2016). In the ampulla, sperm swim away from a fertilized oocyte and enter the cumulus matrix of an unfertilized oocyte (Hino et al., 2016).

Spermiogenesis is dramatic morphological changes of postmeiotic male germ cell, including formation of sperm-specific structures, acrosome and tail (Fig. 2). The acrosome overlying the apical surface of sperm head is an organelle derived from Golgi apparatus. In fertilization, exocytosis of acrosomal components, called acrosome reaction, enabled sperm to penetrate cumulus matrix surrounding oocytes and zona pellucida of oocytes. Reorganization of status in sperm head following the exocytosis is essential to fuse with oocytes. Indeed, only acrosome-reacted sperm are capable of fusing with the oocyte plasma membrane. Our previous study elucidated that the exocytosis of acrosomal components are accelerated by enzymatic activities of serine protease acrosin (ACR) present in the acrosome. Mouse sperm lacking ACR displayed remarkable delays in a dispersal of acrosomal components during acrosome reaction (Yamagata et al., 1998).

Proacrosin-binding protein (ACRBP/sp32) is identified as a binding protein of proacrosin (proACR) which is a zymogen of ACR (Baba et al., 1989; Baba et al., 1994a; Hardy et al., 1991). In mice, alternative splicing of the *Acrbp* pre-mRNA produces wild-type ACRBP-W and variant ACRBP-V5, and both proteins specifically localize in the acrosomal granule (Kanemori et al., 2013). Previously, we reported that male mice lacking both ACRBP-W and ACRBP-V5 showed a significantly reduced

7
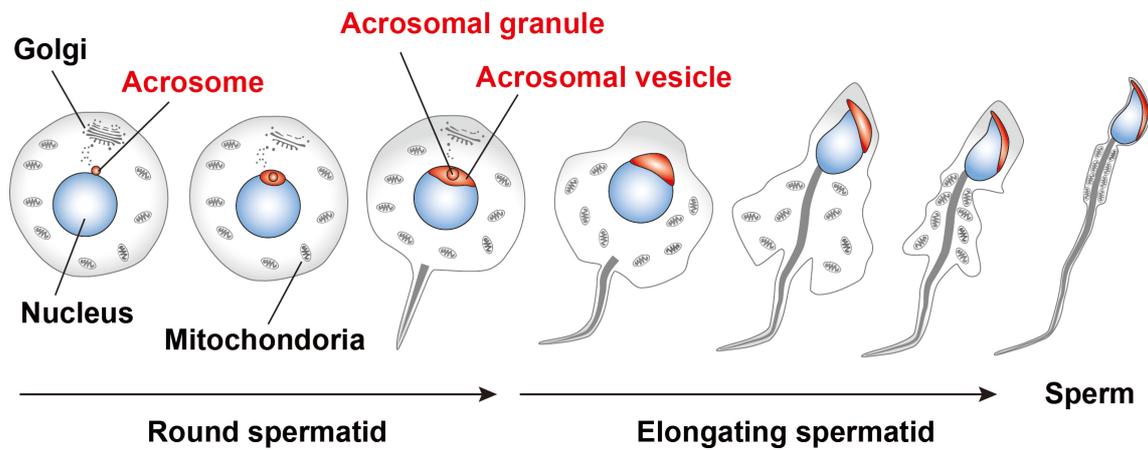
Figure 2. Process of mouse spermiogenesis
During spermiogenesis, male germ cell form sperm-specific organelle, acrosome and tail. At the beginning of round spermatid phase, golgi-derived small vesicles containing hydrolytic enzymes are transported and fused with acrosome sac. As spermiogenesis proceeds, acrosome is elongated and spread over the nucleus.

fertility (Kanemori et al., 2016). Abnormal biogenesis of acrosome in $Acrbp^{-/-}$ sperm results in morphological variations of sperm head. Based on the shapes of the nucleus and acrosome, $Acrbp^{-/-}$ sperm are divided into four groups (types 1, 2, 3, and 4). Type 1 $Acrbp^{-/-}$ sperm contain slightly deformed acrosome on the nucleus essentially similar to that of $Acrbp^{+/+}$ sperm; heads of type 2 and type 3 sperm are moderately and severely affected, respectively; type 4 sperm display a round-headed shape with a coiled midpiece around the nucleus. Morphological abnormalities of cauda epididymal sperm in $Acrbp^{-/-}$ mice influence flagellar bending patterns. When $ACRBP\text{-}V5$ were introduced into $Acrbp^{-/-}$ mice, acrosomal granule is formed during spermiogenesis and sperm morphology is likely to be $Acrbp^{+/+}$ sperm. Moreover, 55- and 53-kDa proACR detected in $Acrbp^{+/+}$ epididymal sperm are mostly processed to 33-kDa mature form of ACR in $Acrbp^{-/-}$ sperm. The aberrant processing of proACR in $Acrbp^{-/-}$ mice are recovered in $Acrbp^{-/-}$ sperm expressing exogenous $Acrbp\text{-}W$. Thus, ACRBP-V5 contribute to the formation and configuration of acrosome granule during spermiogenesis and ACRBP-W maintain proACR as an enzymatically inactive zymogen in the acrosome. Although the functional roles of ACRBPs during spermiogenesis are examined in previous work, the behavior of ejaculated $Acrbp^{-/-}$ sperm in the female reproductive tract remains unclear.

In this study, I have examined the behavior of $Acrbp^{-/-}$ sperm in the female reproductive tract. Analysis of sperm morphology and motility in the uterus and oviduct suggested the presence of sperm selection at the UTJ. Fluorescent labeling of $Acrbp^{-/-}$ sperm by the transgenes exhibited accumulation of sperm within the cumulus matrix surrounding oocytes in the ampulla. Furthermore, incomplete dispersal of acrosomal matrix

components during acrosome reaction was found in $Acrbp^{-/-}$ sperm. On the basis of the data obtained, the cause of subfertility in $Acrbp^{-/-}$ male mice are discussed.

MATERIALS AND METHODS

Animal Experiments

All animal experiments were ethically carried out according to the *Guide for the Care and Use of Laboratory Animals* at University of Tsukuba.

Animals

Mutant $Acrbp^{-/-}$ and $Acr^{-/-}$ mice were generated as described previously (Baba et al., 1994b; Kanemori et al., 2016). $Acrbp^{-/-}$ mice were crossed to transgenic mice (*B6D2F1-Tg [CAG/su9-DsRed2, Acr3-EGFP] RBGS002Osb*), termed Tg^{RBGS} mice, expressing red fluorescent protein (RFP) and green fluorescent protein (GFP) in the mitochondoria and acrosome, respectively (Hasuwa et al; 2010). After the crossbreeding, $Acrbp^{+/+}Tg^{RBGS}$ and $Acrbp^{-/-}Tg^{RBGS}$ mice were backcrossed to Institute of Cancer Research (ICR)-strain mice (Japan SLC, Shizuoka, Japan), and maintained in our laboratory. Mice were genotyped for $Acrbp^{-/-}$, $Acr^{-/-}$ mice and Tg^{RBGS} mice by polymerase chain reaction (PCR) analysis of tail DNAs using the following sets of primers: *Acrbp,* 5'-GTATCCCTTGGACCACTGAAC-3' and 5'-GATCCAACTGAACGAGAGTGG-3'; *Acrbp* mutation, 5'-GTATCCCTTGGACCACTGAAC-3' and 5'-CACTTGTGTAGCGCCAAGTGC-3'; *Acr*, 5'-GTCCTCCCCAAATACCCCA-3' and 5'-TGGGTTATACTTCAGCTCAG-3'; *Acr* mutation, 5'-TTCTATCGCCTTCTTGACGAGTTCT-3' and 5'-TGGGTTCTACTTCAGCTCAG-3'; *Acr3-EGFP*, 5'-GTGGAGCTTTGTGAGGTCACAG-3' and

5'-CAGCTTGCCGGTGGTGCAGATG-3'; *CAG/su9-DsRed2*, 5'-CCTACAGCTCCTGGGCAACGTGC-3' and 5'-AGCCAGAAGTCAGATGCTCAAGGGGC-3'. As an internal control of, another primer set (mLC3ex3GT, 5'-TGAGCGAGCTCATCAAGATAATCAGGT-3' and mLC3ex4AG, 5'-GTTAGCATTGAGCTGCAAGCGCCGTCT-3') was used to amplify the third intron of the LC3 genome in PCR of tail DNAs from Tg[RBGS] mice (Mizushima et al., 2004).

Number of Sperm in the Uterus and Oviduct

ICR mice (8 wk old) were superovulated by intraperitoneal injection of equine chorionic gonadotropin (5 units; ASKA Pharmaceutical, Tokyo, Japan) followed by human chorionic gonadotropin (hCG; 7.5 units; ASKA Pharmaceutical) 48 h later, as described previously (Kawano et al., 2010; Yamashita et al., 2008). Female ICR mice were mated with male mice (3–5 mo old) 12 h after hCG injection. Ejaculated sperm in the uterus were recovered 1.5 h after mating, transferred into a 1.5-ml microtube, measured volume of the fluid, and the number of sperm was counted after dilution in PBS. Sperm in the oviduct were collected by perfusion of PBS on a glass slide 2 h after mating. The oviductal sperm were fixed with 4% paraformaldehyde in PBS (pH 7.2) at room temperature for 30 min, washed with PBS, stained with 0.04% Coomassie brilliant blue (CBB) at room temperature for 10 min, and the sperm number was counted under an IX-71 microscope (Olympus, Tokyo, Japan).

Sperm Morphology

Cauda epididymal sperm were dispersed in a 50-μl drop of TYH (Toyoda et al., 1971) medium free of BSA for 10 min, and capacitated by incubation for 2 h in a 200-μl TYH drop at 37°C under 5% CO_2 in air. Ejaculated sperm in the uterus were recovered 1.5 h after mating, and washed with cold PBS. Sperm in the oviduct were collected by perfusion with PBS on a glass slide 4 h after mating, and dried up at 37°C. The capacitated epididymal sperm, uterine sperm, and oviductal sperm were fixed with 4% paraformaldehyde in PBS, pH 7.2, on ice for 30 min, and washed with PBS. After blocking with PBS containing 3% normal goat serum for 30 min, sperm cells were incubated with Alexa Fluor 568-conjugated peanut agglutinin (PNA; 3 μg/mL; Thermo Fisher Scientific, Waltham, MA), MitoTracker Green FM (2.5 μg/ml; Molecular Probes, Eugene, OR), and Hoechst 33342 (2.5 μg/mL; Thermo Fisher Scientific) for 30 min, washed with PBS, mounted, and then observed under an IX-71 fluorescence microscope (Olympus), as described previously (Yamazaki et al; 2007).

Sperm Motility

Ejaculated sperm in the uterus were recovered 1.5 h after mating and transferred on a prewarmed glass slide. Sperm in the oviduct were collected by perfusion with a 20-μl BSA-free TYH medium on a glass slide 4 h after mating. The aliquot containing the uterine and oviductal sperm were covered with a coverslip and then observed at 37°C by video recording at 200 frames per second under a phase-contrast microscope (Olympus IX-71) equipped with a high-speed camera (HAS-220; Ditect, Tokyo, Japan). Trajectories of sperm were analyzed by a Manual Tracking plugin

of ImageJ software (http://rsbweb.nih.gov/ij/). An apical end of sperm head was tracked at 200 frames per second for 1 second. Parameters of sperm motility were quantified by coordinates of sperm head for 1 second. Following parameters were assessed: curvilinear velocity (VCL, µm/s) calculated by the total distances along the trajectory for collecting time, average path velocity (VAP, µm/s) calculated by average coordinates of sperm from one-sixth (33 frames) of video-frame rates, straight-line velocity (VSL, µm/s) calculated by the straight-line distance between the first and last points of the trajectory for collecting time, linearity (LIN = VSL/VCL, %), straightness (STR = VSL/VAP, %), and wobble (WOB = VAP/VCL, %) (Mortimer, 1997; Wilson-Leedy and Ingermann, 2007).

Sperm Migration through the Oviduct after Mating

Superovulated female mice (8 wk old) were mated with $Acrbp^{+/+}Tg^{RBGS}$ and $Acrbp^{-/-}Tg^{RBGS}$ mice (3–5 mo old) 12 h after the hCG injection. The intact oviduct connecting the uterus was excised from the mice 6 h after mating, placed on a glass slide, and observed at 37°C under an IX-71 fluorescence microscope (Olympus), as described previously (Ishikawa et al., 2016).

Calcium Ionophore-Induced Acrosome Reaction

Capacitated epididymal sperm (4×10^6 sperm/ml) in a 200-µl TYH drop were induced to undergo acrosome reaction by addition of calcium ionophore A23187 (Sigma-Aldrich, St. Louis, MO) at a final concentration of 20 µM followed by incubation at 37°C under 5% CO_2 in air for 1 h.

After incubation, sperm cells were transferred into a 1.5-ml microtube, washed with PBS, fixed with 4% paraformaldehyde in PBS on ice for 15 min, stained with 0.04% CBB at room temperature for 5 min, washed with PBS, and viewed under an IX-71 microscope (Olympus), as described previously (Yamashita et al., 2008). Sperm were also immunoreacted with anti-IZUMO1 (Inoue et al., 2005) antibody, incubated with Alexa Fluor 488-conjugated antibody against rabbit IgG, counterstained with Hoechst 33342, and observed.

Cumulus Cell Dispersal Assay

After capacitation of cauda epididymal sperm in a 200-μl TYH drop, swim-up sperm (1.5×10^4 sperm/10 μl) were mixed with the OCCs in a 90-μl TYH drop. The mixture (100 μl) was incubated at 37°C under 5% CO_2 in air, and then observed under an IX-71 microscope, as described previously (Kimura et al., 2009).

Statistical Analysis

The Student *t*-test was used for statistical analysis; significance was assumed for *P* < 0.05.

RESULTS

Distribution of ACRBP-Deficient Sperm in the Female Reproductive Tract

To examine the presence of sperm in the female reproductive tract after ejaculation, wild-type female mice were mated with $Acrbp^{+/+}$ and $Acrbp^{-/-}$ male mice. The ejaculated sperm in the uterus and oviduct were counted 1.5 and 2 h after mating, respectively (Fig. 3, A and B). No significant difference of sperm number between $Acrbp^{+/+}$ and $Acrbp^{-/-}$ mice was found in the uterus. However, the oviduct contained much smaller number of $Acrbp^{-/-}$ sperm (approximately 120 cells) than that of $Acrbp^{+/+}$ sperm (>400 cells). These data suggest inefficient migration of $Acrbp^{-/-}$ sperm from the uterus to oviduct through UTJ.

As described previously (Kanemori et al., 2016), the whole population of $Acrbp^{-/-}$ sperm in cauda epididymis were divided into four cell types (types 1, 2, 3, and 4) based on the shapes of nucleus and acrosome (Fig. 3C). I asked whether the morphological differences of $Acrbp^{-/-}$ sperm were involved in the decrease of sperm number in the oviduct. By staining of nucleus, acrosome, and mitochondoria, the ratios of type 1, type 2, type 3, and type 4 epididymal sperm from $Acrbp^{-/-}$ mice were found to be 46, 37, 15, and 2% (53, 37, 8, and 1% for the uterine sperm), respectively (Fig. 3D). Compared with epididymal sperm, the ratio of type 3 $Acrbp^{-/-}$ sperm was slightly decreased in the uterus, despite no significant differences in the other types. More than 80% of sperm were classified into type 1 in the oviduct, whereas the ratios of type 2 and type 3 were approximately 15% and 3%, respectively. No type 4 sperm was observed in the oviduct. Thus, $Acrbp^{-/-}$ sperm possessing morphologically

16
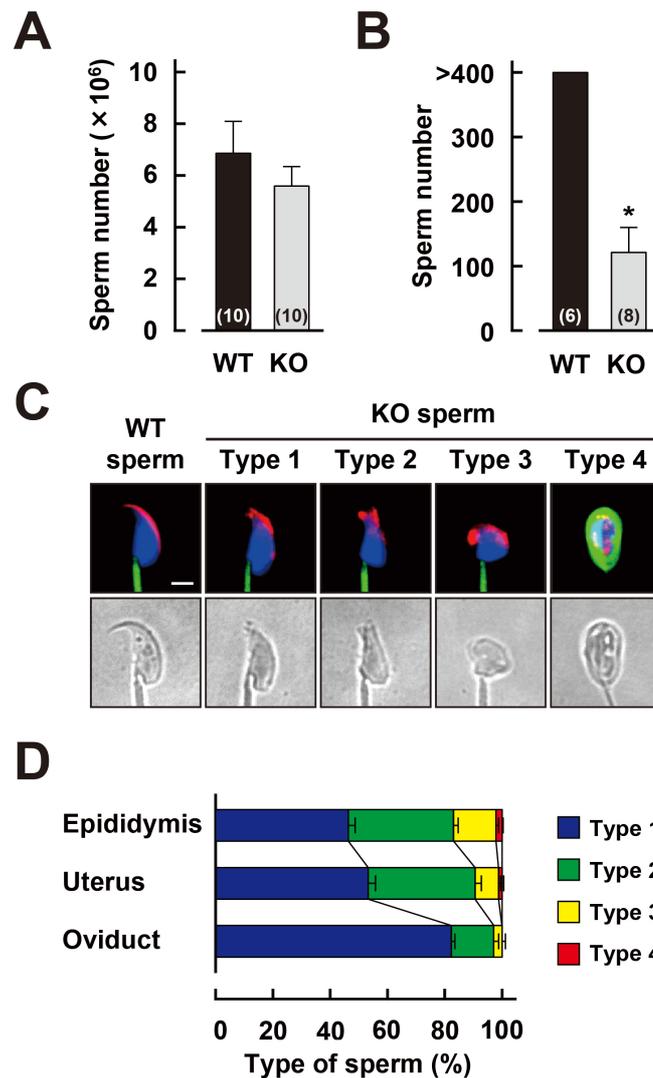
Figure 3. Morphological distribution of ACRBP-deficient sperm
A and B) Sperm number in the uterus and oviduct. Uterine sperm were recovered 1.5 h after mating, and then counted (A). The oviduct were dissected 2 h after mating. Oviductal sperm were collected by PBS perfusion, stained with Coomassie brilliant blue, and then counted (B). **$P < 0.01$. Total number of uterus and oviduct are indicated in parentheses. **C)** Sperm morphology. Cauda epididymal sperm of wild-type (WT) and ACRBP-deficient (KO) mice were capacitated by incubation for 2 h in a TYH drop. After fluorescent staining, KO sperm were morphologically divided into four types. The acrosome, midpiece, and nucleus were stained with fluorescent dye-labeled PNA (red), mitotracker (green), and Hoechst 33342 (blue), respectively. Scale bar = 4 μm. **D)** Typing of KO sperm by head morphology. Ejaculated KO sperm were recovered from the uterus and the oviduct 1.5 and 4 after mating, respectively. More than 200 sperm were randomly selected and counted for epididymal and uterine sperm, and more than 100 sperm were counted for oviductal sperm. The differences in ratios of sperm type are significant between epididymal and uterine type 3 sperm, between uterine and oviductal type 1 sperm, between uterine and oviductal type 2 sperm, and between uterine and oviductal type 3 sperm ($P < 0.01$).

normal shape of the head may preferentially pass through the UTJ.

Involvement of Sperm Motility in Migration through the UTJ

I examined whether motility of $Acrbp^{-/-}$ sperm were also involved in migration from the uterus to oviduct through UTJ. Motile uterine sperm recovered 1.5 h after mating were recorded by a high-speed camera, and then apical end of sperm heads were tracked by ImageJ software (Fig. 4A). It should be noted that type 1 $Acrbp^{-/-}$ sperm was morphologically indistinguishable from type 2 sperm under bright-field conditions. The type 1/type 2 sperm showed a transient irregular movement or frequent side-to-side head movement unlike $Acrbp^{+/+}$ sperm. Swimming distances of type 3 and type 4 sperm were quite short due to the reduction of velocities. The obtained sperm trajectories were quantified using the parameters in Computer-assisted semen analysis (CASA). Following parameters were assessed: curvilinear velocity (VCL, μm/s) calculated by the total distances along the trajectory for collecting time, average path velocity (VAP, μm/s) calculated by average coordinates of sperm from one-sixth (33 frames) of video-frame rates, straight-line velocity (VSL, μm/s) calculated by the straight-line distance between the first and last points of the trajectory for collecting time, linearity (LIN = VSL/VCL, %), straightness (STR = VSL/VAP, %), and wobble (WOB = VAP/VCL, %). Type 1/type 2 sperm exhibited the scores of velocities (VCL, VSL, and VAP) and straightness (STR) similar to those of $Acrbp^{+/+}$ sperm, whereas the scores of linearity (LIN) and wobble (WOB) were significantly reduced (Fig. 4B). These data indicated that swimming patterns of type 1/type 2 sperm differed from $Acrbp^{+/+}$ sperm without the reduction of velocities. All parameters except

18
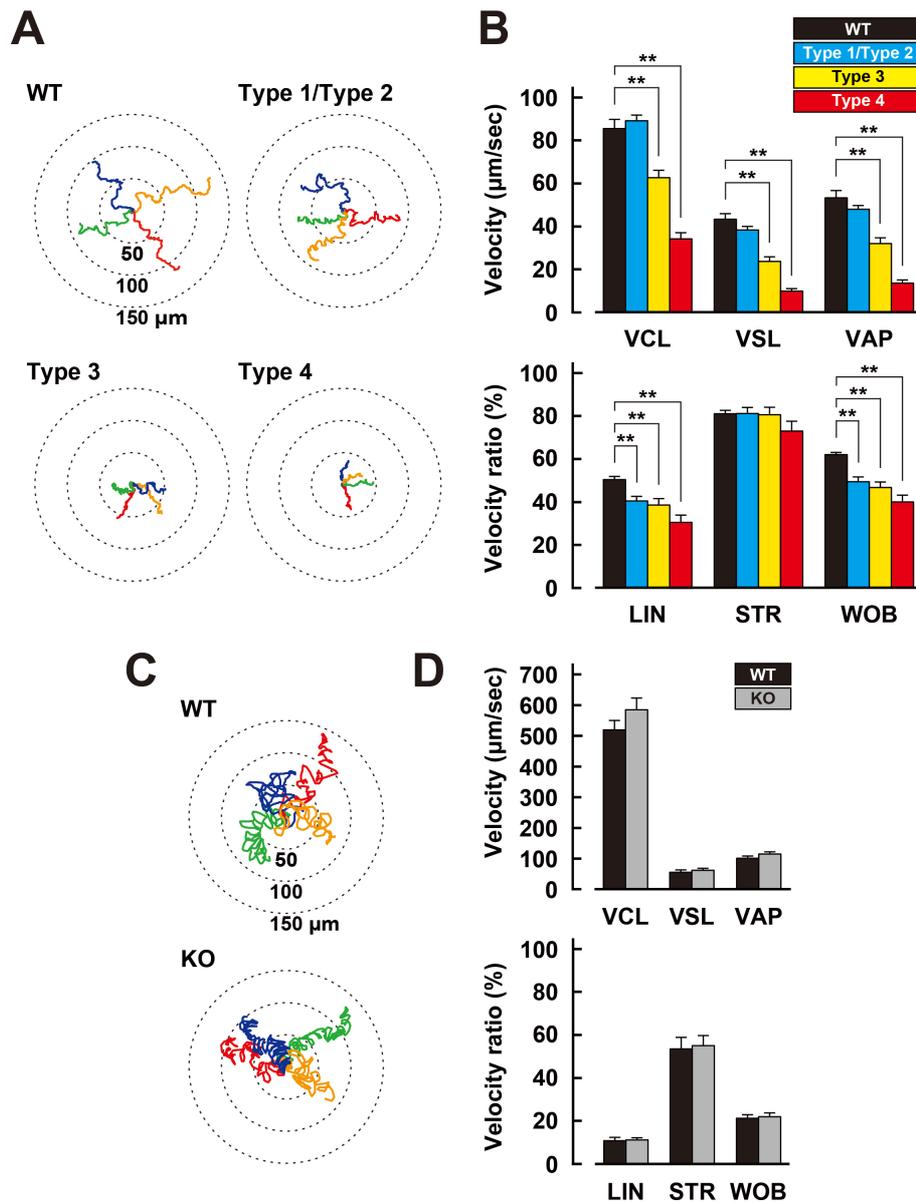
**Figure 4. Motility pattern of uterine and oviductal sperm**
A) Trajectories of representative sperm cell types in the uterus. Uterine sperm were collected 1.5 h after mating and monitored by video recording at 200 frames/second with a high-speed camera. Motile sperm were tracked by Manual tracking/ImageJ for 1 second (equal to 200 flames). Type 1 KO sperm were indistinguishable from type 2 sperm under bright field condition. **B)** Parameters of uterine sperm motility. The parameters were calculated from the trajectories of uterine sperm. VCL, curvilinear velocity; VAP, average path velocity; VSL, straight-line velocity; LIN, linearity; STR, straightness; and WOB, wobble. A total of 30, 76, 46, and 31 sperm were examined for WT, type 1/type 2, type 3, and type 4 KO sperm, respectively. **$P < 0.01$. **C)** Trajectories of representative sperm cell types in the oviduct. Following mating, sperm in the oviduct were collected by perfusion of BSA-free TYH medium 4 h after mating, and then monitored. **D)** Parameters of oviductal sperm motility. A total of 30 sperm each were examined for WT and KO sperm.

STR were reduced moderately and severely in type 3 and type 4 sperm, respectively. Thus, motilities of type 3 and type 4 sperm in the uterus were dysfunctional.

I collected $Acrbp^{-/-}$ sperm in the oviduct 4 h after mating and analyzed the motility (Fig. 4, C and D). As described in Fig. 3D, the population of $Acrbp^{-/-}$ sperm in the oviduct was predominantly type 1/type 2 (97%). The collected $Acrbp^{+/+}$ and $Acrbp^{-/-}$ sperm from the oviduct displayed hyperactivation-like trajectories. Examined parameters, including LIN and WOB, of $Acrbp^{-/-}$ sperm in the oviduct were comparable to those of $Acrbp^{+/+}$ sperm. Thus, $Acrbp^{-/-}$ sperm present in the oviduct possess nearly equal motility to $Acrbp^{+/+}$ sperm. Considering the various patterns of motility in the uterine $Acrbp^{-/-}$ sperm, the observations in the oviduct suggest the sperm were also selected by motility in the UTJ.
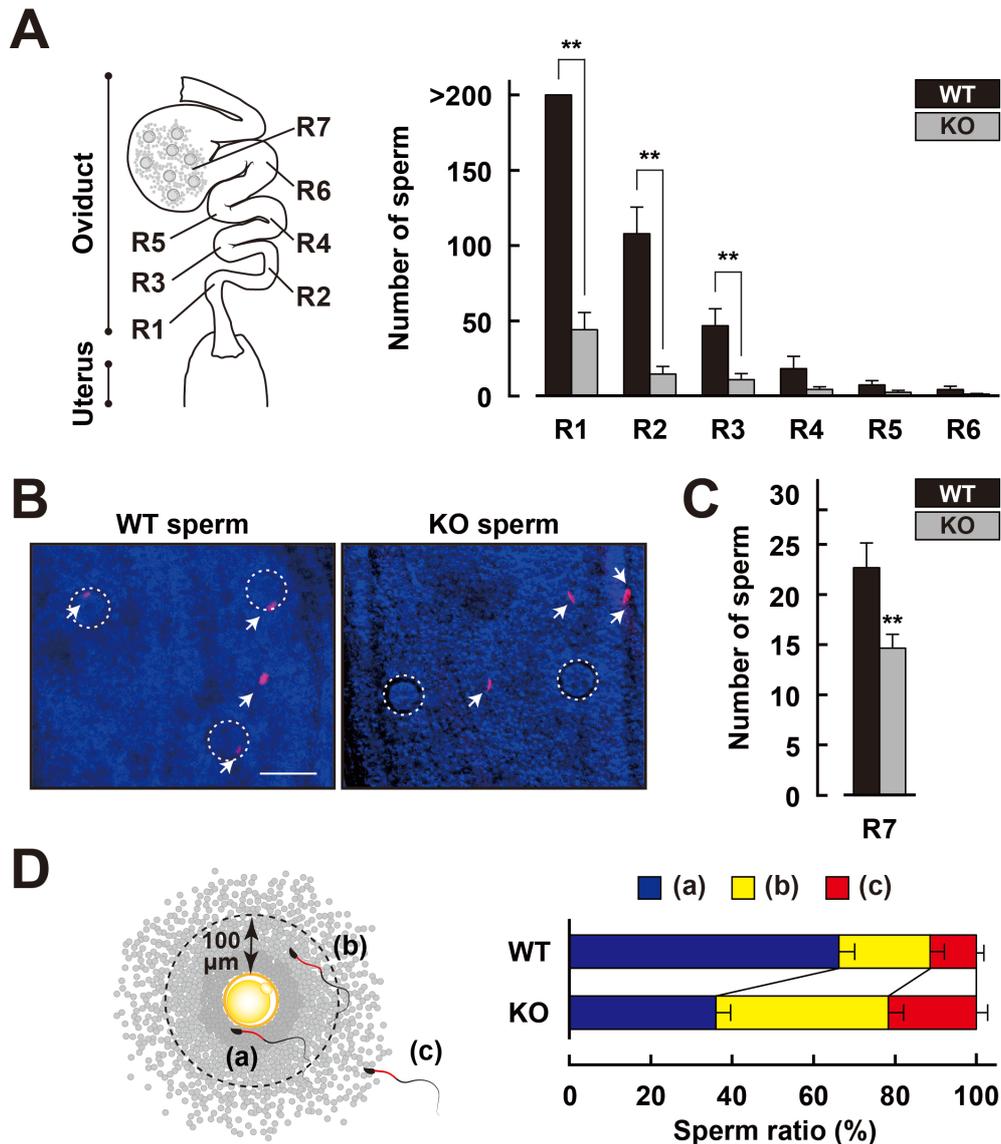
Accumulation of ACRBP-Deficient Sperm within the Cumulus Matrix

To visualize sperm migration in the oviduct, transgenes expressing green fluorescent protein (GFP) and red fluorescent protein (RFP) in the acrosome and mitochondria, respectively, termed Tg^{RBGS} (Hasuwa et al., 2010), were introduced into $Acrbp^{-/-}$ mice (Fig. 5, A and B). After mating of $Acrbp^{+/+}Tg^{RBGS}$ and $Acrbp^{-/-}Tg^{RBGS}$ mice to wild-type female mice, the oviducts were dissected and observed under a fluorescence microscope. I divided the oviduct into seven regions (R1–R7), where the isthmus corresponds to R1 and R2, and the ampulla corresponds to R7, and counted the sperm number in each region (Fig. 6A). More than 200 $Acrbp^{+/+}Tg^{RBGS}$ sperm in R1 were observed, and the sperm number was gradually decreased toward R7. Compared with $Acrbp^{+/+}Tg^{RBGS}$ sperm, significant
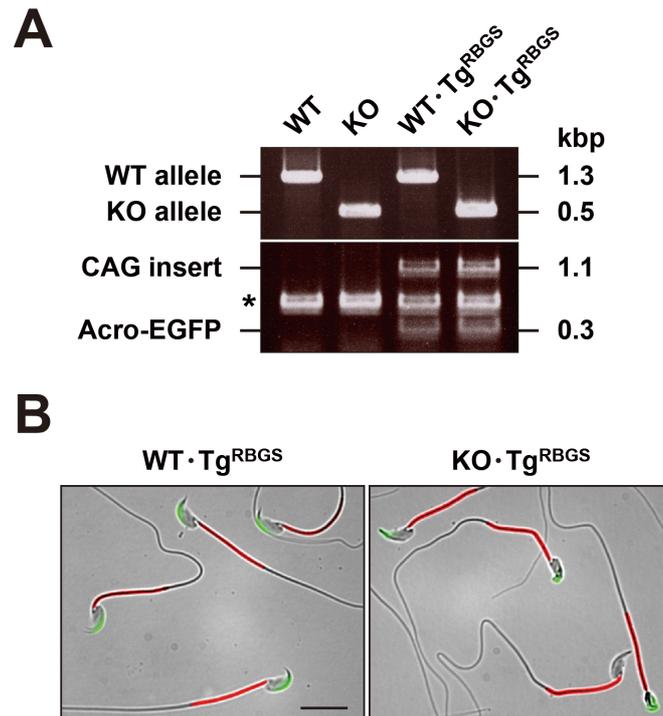
Figure 5. Introduction of transgenes into ACRBP-deficient mice

A) Agarose gel electrophoresis of PCR product. Transgenic mice (*B6D2F1-Tg [CAG/su9-DsRed2, Acr3-EGFP] RBGS002Osb*), termed Tg^RBGS mice, expressing GFP in the acrosome and RFP in the mitochondria were mated with ACRBP-deficient (KO) sperm mice. PCR was carried out using tail genomic DNAs. CAG/su9-DsRed2 and Acr3-EGFP were also examined by PCR analysis. Asterisk indicate bands of internal control (LC3). **B)** Cauda epididymal sperm from WT and KO mice. The transgenic sperm expressing GFP (green) and RFP (red) in acrosome and mitochondoria, respectively. Scale bar = 20 μm.

Figure 6. Localization of ACRBP-deficient sperm in the oviduct

A) Regional distribution of sperm in the oviduct. Superovulated female mice were mated with wild-type (WT) and ACRBP-deficient (KO) mice expressing fluorescent proteins. The number of sperm at R1–R6 were counted 6 h after mating. Eight oviducts each were examined for WT and KO sperm. *$P < 0.05$; **$P < 0.01$. **B)** Observation of sperm in the ampulla (R7). The region surrounded by dot circle indicates an oocyte. Sperm are indicated by arrows. Asterisks indicate the non-specific fluorescence. Scale bar = 100 μm. **C)** Sperm number in the ampulla. The number of sperm at R7 was counted 6 h after mating. Fifteen oviducts each were examined for WT and KO sperm. **$P < 0.01$. **D)** Classification of sperm localization in the ampulla. The localization of sperm was defined as pattern a, b, and c. Sperm on zona pellucida (ZP) of the oocyte, sperm within the range of 100 μm distance from the ZP (dotted circles), and sperm outside of the 100 μm distance from the ZP were corresponding to pattern a, b, and c, respectively. Fifteen oviducts each were examined for WT and KO sperm. The differences in ratios of sperm type are significant between WT and KO pattern a, between WT and KO pattern b, and between WT and KO pattern c, respectively ($P < 0.01$).

decreases in $Acrbp^{-/-}Tg^{RBGS}$ sperm were found at R1–R3, but not R4–R6. When observed at R7, approximately 22 $Acrbp^{+/+}Tg^{RBGS}$ sperm and 14 $Acrbp^{-/-}Tg^{RBGS}$ sperm were located adjacent to the oocyte-cumulus complexes (OCCs) (Fig. 6, B and C). This data suggests that the number of $Acrbp^{-/-}Tg^{RBGS}$ sperm reaching the ampulla is smaller than that of $Acrbp^{+/+}Tg^{RBGS}$ sperm.

$Acrbp^{-/-}Tg^{RBGS}$ sperm displayed unique localization surrounding the OCCs in addition to the smaller number (Fig. 6B). Although most of $Acrbp^{+/+}Tg^{RBGS}$ sperm attached on surface of the zona pellucida (ZP) at R7, localization of $Acrbp^{-/-}Tg^{RBGS}$ sperm appeared to be away from ZP. I divided the localization of sperm at R7 into three types: sperm on ZP, sperm within the cumulus matrix, and sperm outside the cumulus matrix. The ratios of sperm on ZP, within the cumulus matrix, and outside the cumulus matrix were ~66, 23, and 11%, respectively, in $Acrbp^{+/+}Tg^{RBGS}$ mice (Fig. 6D). Interestingly, the ratio of $Acrbp^{-/-}Tg^{RBGS}$ sperm was decreased on ZP (36%) and increased within the cumulus matrix (42%), implying the impaired ability of sperm penetration through the cumulus matrix. These results suggest that decreased sperm number and unusual sperm localization in the ampulla may be leading causes of the severely reduced fertility in $Acrbp^{-/-}$ male mice.

Requirement of ACRBP for the Acrosome Reaction and Dispersal of Cumulus Cells

Dispersal of acrosomal protein during the acrosome reaction assists sperm penetration through the cumulus matrix (Kawano et al., 2010; Zhou et al., 2012). I attempted to evaluate the status of the acrosome reaction *in*

vivo, but collecting sperm from the ampulla was technically difficult. To assess the ability of acrosome reaction in *Acrbp*$^{-/-}$ sperm *in vitro*, cauda epididymal sperm were capacitated and then induced acrosome reaction by calcium ionophore A23187. After treating with A23187, the acrosome reaction was examined by staining with Coomassie brilliant blue (CBB) and anti-IZUMO1 (Inoue et al., 2005) antibody (Fig. 7, A and B). Although acrosomal proteins were completely dispersed in 81% of *Acrbp*$^{+/+}$ sperm, CBB-stained acrosomes were remained in 61% of *Acrbp*$^{-/-}$ sperm (Fig. 7C). Sperm containing the IZUMO1-positive signal on the entire head region were counted as acrosome-reacted sperm (Kawano et al., 2010). The rate of A23187-induced acrosome reaction was moderately decreased in the whole population of *Acrbp*$^{-/-}$ sperm, compared with that of *Acrbp*$^{+/+}$ sperm. When the whole population of *Acrbp*$^{-/-}$ sperm was divided into the morphological types, acrosome-reacted type 1 and type 2 sperm were remarkably decreased in the both staining of CBB and anti-IZUMO1 antibody compared with *Acrbp*$^{+/+}$ sperm. In addition, there was a significance in the acrosome reaction rate detected by IZUMO1 between type 2 and type 3 sperm. Thus, defects in the acrosome reaction and dispersal of acrosomal proteins were more evident according to the sperm-head abnormalities (Fig. 7D).

Furthermore, I examined whether the defective acrosome reaction in *Acrbp*$^{-/-}$ sperm affected to dispersal of cumulus cells. After capacitated *Acrbp*$^{+/+}$ and *Acrbp*$^{-/-}$ sperm were mixed with the OCCs, the status of cumulus cells were monitored over 6 h (Fig. 8A). Cumulus cells without sperm were gradually broken away from the OCCs, presumably due to cumulus matrix loosening (Florman and Ducibella., 2006). The status was defined as three patterns if the oocytes were surrounded by approximately
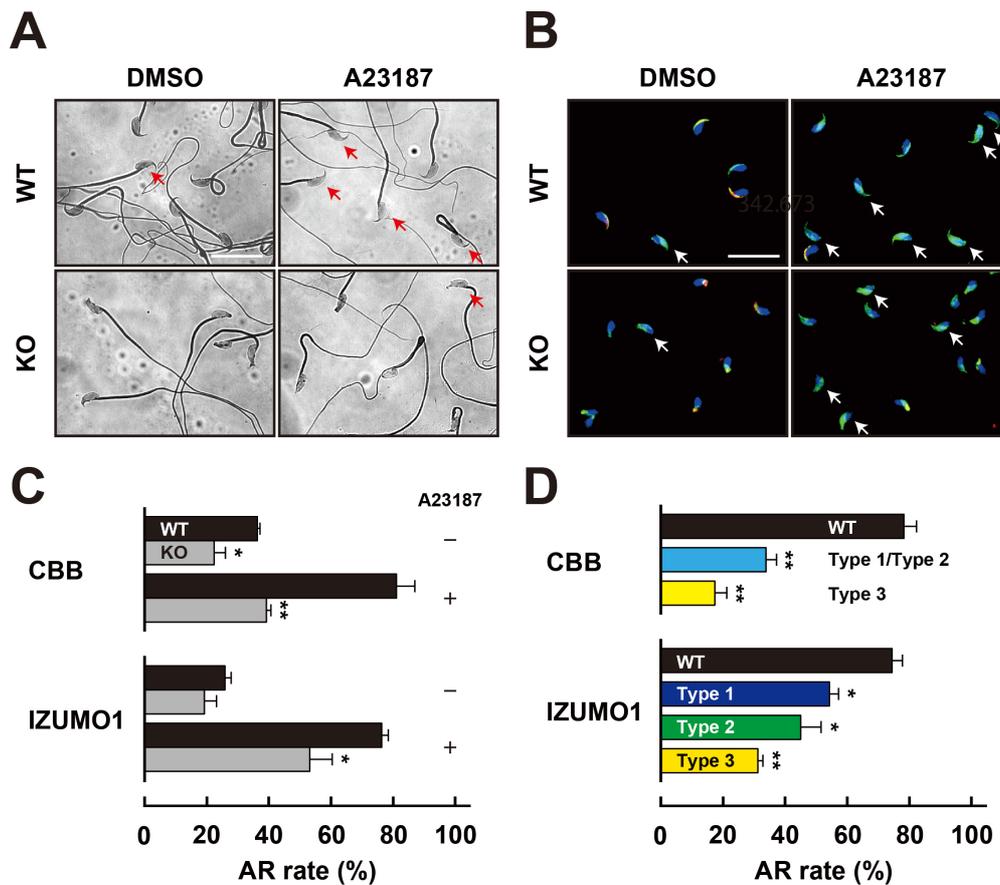
Figure 7. A23187-induced acrosome reaction of cauda epididymal sperm
A and B) Acrosome reaction induced by calcium ionophore A23187. Capacitated cauda epididymal sperm from wild-type (WT) and ACRBP-deficient (KO) mice were treated with dimethyl sulfoxide (DMSO) or 20 μM calcium ionophore A23187, and stained by Coomassie brilliant blue (CBB) (A) and anti-IZUMO1 antibody (B). Arrows indicate the acrosome-reacted (AR) sperm. Scale bar = 50 μm. **C)** The rates of acrosome-reacted (AR) sperm after A23187 treatment. The 200 sperm were selected at random and AR sperm were counted (n = 3). **D)** Comparison of AR sperm rate in morphological types of KO sperm. Following morphological classification, the 100 sperm were selected at ramdom and counted for each types. Note that acrosome status of type 4 sperm was visually undetectable because of round-headed shape with a coiled midpiece. Type 1 KO sperm was morphologically indistinguishable from type 2 sperm under bright-field conditions after CBB staining. *$P < 0.05$; **$P < 0.01$.
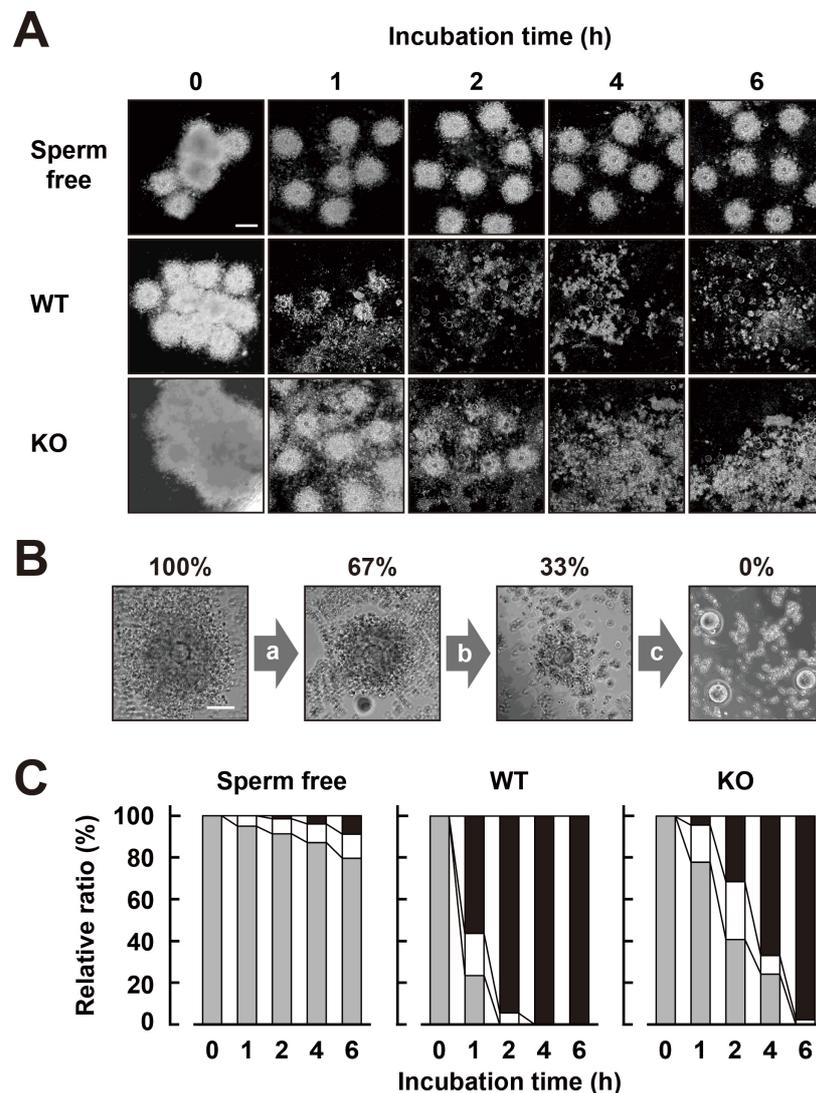
Figure 8. Dispersal of cumulus cells from the OCC
A) Time course of cumulus cell dispersal. Capacitated epididymal sperm from wild-type (WT) and ACRBP-deficient (KO) mice were mixed with the oocyte cumulus complexes (OCCs) at a concentration of 150 sperm/μl. After incubation, the OCCs were observed under a microscope. As a control, the OCCs were also incubated in the absence of sperm as a control (Sperm free). Scale bar = 500 μm. **B)** Criterion of the oocyte status. The status was defined as patterns a, b, and c when the oocytes were surrounded by approximately 0–33%, 34–67%, and 68–100% of cumulus cells, respectively. Scale bar = 100 μm. **C)** Delayed cumulus cell dispersal by KO epididymal sperm. The OCCs were inseminated by capacitated epididymal sperm as described above, and the oocyte status (lightly shaded, open, and closed boxes for patterns a, b, and c, respectively) was assessed at time intervals indicated (*n* = 3). A total of 82 and 66 oocytes were examined for WT and KO sperm, respectively (57 oocytes for sperm free).

26

0–33%, 34–67%, and 68–100% of original cumulus cells, respectively (Fig. 8, B and C). Almost all oocytes lost cumulus cells 2 h after incubation with *Acrbp*$^{+/+}$ sperm. Dispersal of cumulus cells were apparently delayed by the presence of *Acrbp*$^{-/-}$ sperm. Some oocytes were still surrounded with cumulus cells even 4 h after incubation. These observations suggest that defective dispersal of acrosomal proteins in *Acrbp*$^{-/-}$ sperm may result in the retention of cumulus cells in the OCCs.

DISCUSSION

This study describes how ACRBP-deficient mouse sperm migrate in the female reproductive tract. My data suggest the presence of sperm selection by morphology and motility at the UTJ during sperm migration from the uterus to oviduct (Figs. 3 and 4). The concept of sperm selection has been proposed using various approaches, including artificial insemination of uncapacitated or capacitated sperm and homologous or heterologous sperm (Shalgi et al., 1992; Smith et al., 1988). Regarding sperm morphology, it has been reported that the UTJ function as a barrier against abnormal sperm carrying severely deformed head (Krzanowska., 1974). The finding supports my results that type 3/type 4 sperm were not allowed to pass through the selection (Fig. 3). Noteworthy is that approximately 15% of sperm in the oviduct were type 2 sperm which have a moderately deformed head. Thus, the UTJ may not strictly select sperm by morphological abnormalities of head. Moreover, gene-knockout strategy in mice revealed that the proper distribution of a disintegrin and metalloproteinase 3 (ADAM3) on sperm surface is essential for sperm migration through the UTJ (Yamaguchi et al., 2006; Yamaguchi et al., 2009). By immunoblot analysis, same levels of ADAM3 protein were found in $Acrbp^{+/+}$ and $Acrbp^{-/-}$ epididymal sperm (Kanemori et al., 2016). If ACRBP interact with ADAM3, migration of $Acrbp^{-/-}$ sperm through the UTJ may be impaired due to abnormal molecular function. Perhaps, ADAM3 caused by abnormal biogenesis of acrosome in $Acrbp^{-/-}$ sperm, especially type 3 and type 4, may affect migration through the UTJ.

I also suggested the presence of sperm selection by motility at the UTJ using CASA parameters (Fig. 4). As reported previously, linear

swimming pattern rather than circular swimming pattern is thought to be required for migration through the UTJ (Gaddum-Rosse., 1981; Shalgi et al., 1992). Despite straightforward swimming, uterine type 1/type 2 $Acrbp^{-/-}$ sperm exhibited irregular swimming patterns, such as a frequent beating and unexpected changes of direction and swimming speed. The characteristic swimming pattern of type 1/type 2 sperm were confirmed by high STR and by low LIN and WOB in the CASA scores. Since the CASA scores of $Acrbp^{-/-}$ sperm (almost all type 1/type 2) were comparable to those of $Acrbp^{+/+}$ sperm in the oviduct, subpopulation of type 1/type 2 sperm with the irregular swimming patterns may be blocked by the UTJ (Fig. 9A).

Differences of shapes and dimensions in sperm head produce various swimming patterns. In red deer, sperm with elongated head statistically swim faster (Gomendio et al., 2007). Fluid mechanical analysis suggested that head dimension of human sperm was one of the factors to determine the straight-line velocity and lateral movement of head (Gillies et al., 2009). Since ACRBP are specifically present in the sperm acrosome, dysfunction of motility may be a secondary effects of abnormal head morphology (Kanemori et al., 2016). Indeed, swimming pattern and CASA scores were altered in $Acrbp^{-/-}$ sperm depending on four morphological types. Motility of type 3 and type 4 sperm which have a severely deformed head was apparently dysfunctional. A clue about the relationship between sperm motility and the selection at the UTJ are provided from the study of mice lacking one of catalytic subunit PPP3CC of Ca^{2+} and calmodulin-dependent serine-threonine phosphatase calcineurin ($Ppp3cc^{-/-}$ mice). Male infertility of $Ppp3cc^{-/-}$ mice is attributed to aberrant flagellar bending patterns of sperm without morphological abnormalities (Miyata et
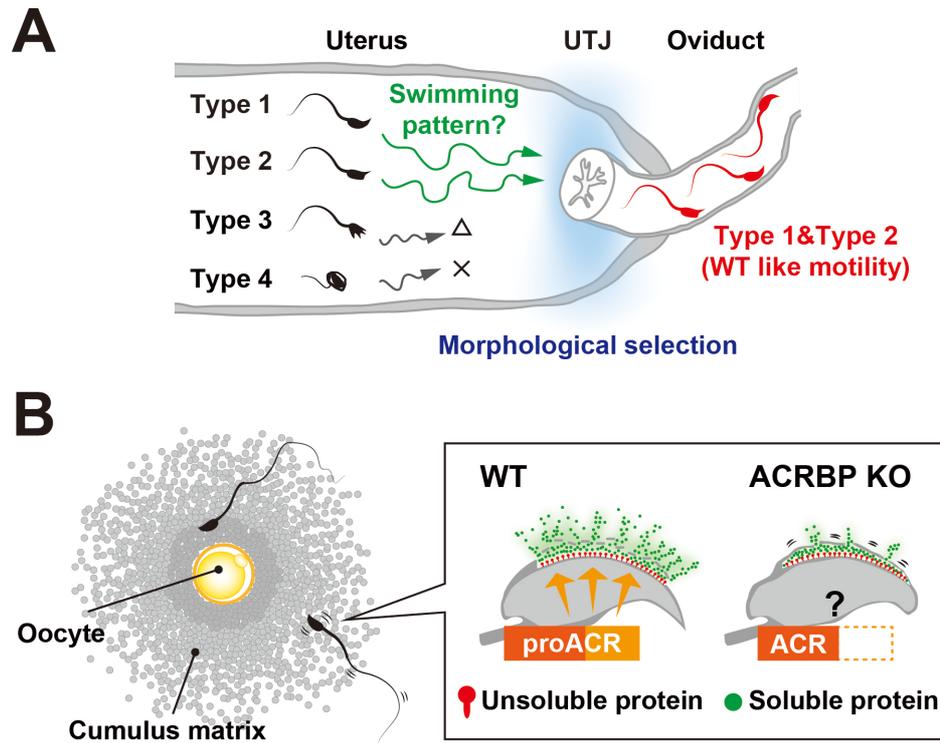
Figure 9. A schematic model for migration of ACRBP-deficient sperm in the female reproductive tract

A) Sperm morphology and motility in sperm selection at the UTJ. Type 1 and type 2 ACRBP-deficient (KO) sperm possessing linear motility without irregular swimming pattern may migrate through the UTJ. Type 3 and type 4 sperm possessing severe morphological abnormalities in head may be blocked by the UTJ due to low velocities. Slight deformation of head, such as type 1 and type 2 sperm, have little effect on the sperm selection at the UTJ. **B)** Sperm/cumulus penetration assisted by acrosome reaction. Dispersal of acrosomal components in ACR KO sperm cause delay in sperm/cumulus penetration (Zhou et al., 2012). Incomplete acrosome reaction in ACRBP KO sperm may result in the accumulation of sperm within the cumulus matrix in the ampulla.

al., 2015). The number of $Ppp3cc^{-/-}$ sperm migrating through the UTJ is much smaller than those of $Ppp3cc^{+/+}$ sperm, suggesting the requirement of motility in the sperm selection. At any rate, both of sperm morphology and motility are important factors to pass through the UTJ.

I analyzed sperm motility with the high-speed camera and ImageJ software because of two reasons. First, morphological classification of $Acrbp^{-/-}$ sperm is technically limited under CASA system. Second, collected oviductal fluids containing a small number of sperm and a lot of debris were unsuitable for CASA system. Motility analysis using high-speed camera (200 fps) enabled us to examine the subtle differences between $Acrbp^{+/+}$ sperm and type 1/type 2 $Acrbp^{-/-}$ sperm. Recently, Wang *et al.* developed a system of optical coherence tomography and perform *in vivo* three-dimensional tracking of sperm behaviors in the mouse oviduct (Wang and Larina., 2018). Such a novel approach help us to elucidate behavioral differences between wild-type and gene knockout mouse sperm in the oviduct lumen in the future.

In the ampulla, oocytes are fertilized one by one by small numbers of sperm for efficient fertilization 4 h after mating (Muro et al., 2016). The number of $Acrbp^{-/-}$ sperm (approximately 14 cells) was unexpectedly greater than the number of oocytes (approximately 13 cells) 6 h after mating (Fig. 6 and Fig. 10A). If all of those sperm fertilize with oocytes, subfertility in $Acrbp^{-/-}$ mice may be unexplained. Accumulation of $Acrbp^{-/-}$ sperm within the cumulus matrix suggested the defects of sperm/cumulus penetration ability. I suspected the possible involvement of acrosin (ACR) in the cumulus penetration (Fig. 9B). Depletion of ACR impaired sperm/cumulus penetration ability due to the delay in dispersal of acrosomal matrix components (Kawano et al., 2010; Yamagata et al., 1998;

31
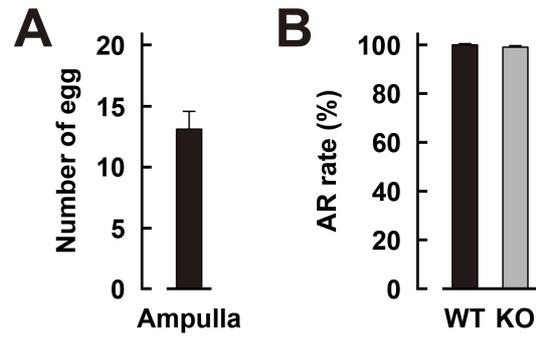
Figure 10. Observations of oocytes and sperm acrosome reaction in the ampulla
A) The number of oocytes in the ampulla. The number of oocytes in superovulated female mice was counted 6 h after mating with wild-type (WT) and ACRBP-deficient (KO) mice expressing fluorescent proteins. Fifteen oviducts each were examined for WT and KO sperm. **B)** Acrosomal GFP of the transgenic sperm in the ampulla. Transgenic sperm which released acrosomal GFP from acrosome were defined as acrosome-reacted (AR) sperm. Fifteen oviducts each were examined for WT and KO sperm.

Zhou et al., 2012). Interestingly, proACR was mostly processed into a mature form of ACR in $Acrbp^{-/-}$ sperm (Kanemori et al., 2016). An aberrant processing of proACR may inhibit the dispersal of acrosomal matrix components in $Acrbp^{-/-}$ sperm (Fig. 7). My additional experiment using $Acr^{-/-}$ mouse sperm confirmed the lower ability to disperse cumulus cells (Fig. 11). Dispersal of cumulus cells was also delayed by the presence of $Acr^{-/-}$ rat sperm (Isotani et al., 2017). Further study is necessary to elucidate the function of ACR in $Acrbp^{-/-}$ mice in the sperm/cumulus penetration. Another possibility for the defects of cumulus penetration ability in $Acrbp^{-/-}$ sperm is dysfunction in chemotaxis system. Sulfated steroid, identified as sperm-activating and -attracting factor (SAAF), released from the ascidian egg activates and then attract sperm toward the egg (Yoshida et al., 2002). In mammals, progesterone and odorant receptors have been reported to function in sperm chemotaxis, but the molecular mechanism remains unclear (Fukuda et al., 2004; Lishko et al., 2011; Spehr et al., 2003; Strunker et al., 2011). If abnormal biogenesis of acrosome in $Acrbp^{-/-}$ sperm affects receptors of chemoattractants, sperm may not recognize the oocyte easily in the ampulla. Although ACRBP protein does not contain functional domains (Kanemori et al., 2013), binding partners of ACRBP except for proACR were not identified at present. Previous study reported that expression level of seven proteins (ZPBP1, ZPBP2, IZUMO1, ADAM3, SPAM1, HYAL5, and PRSS21) involved in fertilization were similar between $Acrbp^{+/+}$ and $Acrbp^{-/-}$ sperm. To examine further the functional role of ACRBP in fertilization, omics approaches including proteome and transcriptome analysis may be required. It should be noted that almost all of the transgenic sperm in the ampulla dispersed acrosomal GFP which is composed of soluble components in
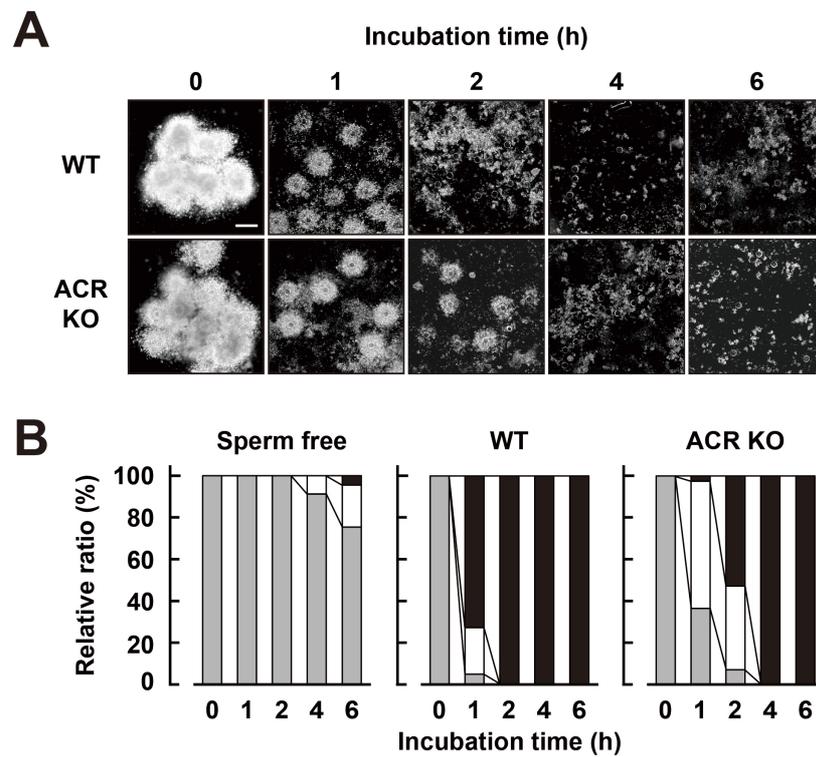
Figure 11. Dispersal of cumulus cells from the OCC by ACR-deficient mouse sperm.
A) Time course of cumulus cell dispersal. Capacitated epididymal sperm from wild-type (WT) and ACR-deficient (KO) mice were mixed with the OCCs at a concentration of 150 sperm/μl. After incubation, the OCCs were observed under a microscope. Scale bar = 500 μm. **B)** Delayed cumulus cell dispersal of ACR KO epididymal sperm. The OCCs were inseminated by capacitated epididymal sperm as described above, and the oocyte status (lightly shaded, open, and closed boxes for patterns a, b, and c, respectively) was assessed at time intervals indicated (*n* = 3). Total numbers of 138 and 140 oocytes were examined for WT and ACR KO sperm, respectively (61 oocytes for sperm free).

acrosome (Fig. 10B) (Hirohashi et al., 2015). Although the disappearance of acrosomal GFP is useful marker for status of soluble proteins, following events, including dynamic diffusion of IZUMO1 and dispersal of acrosomal matrix components, are undetectable (Buffone et al., 2008; Kim et al., 2003; Satouh et al., 2012). Therefore, *in vitro* experiments using calcium ionophore A23187 were an effective approach to examine the status of acrosomal matrix components during acrosome reaction.

My present study suggests that the morphologically abnormal sperm produced in *Acrbp*$^{-/-}$ mice may be underwent sperm selection in the UTJ entry. Moreover, incomplete release of acrosomal matrix components during acrosome reaction may impair the ability of sperm/cumulus penetration ability in *Acrbp*$^{-/-}$ sperm. In the female reproductive tract, differences between sperm selected to fertilize with oocyte and other unfertilized sperm are still open question. I believe that these findings will be informative to elucidate the whole mechanism of the sperm migration in the female reproductive tract in the future.

REFERENCES

Baba T, Michikawa Y, Kashiwabara S, Arai Y. Proacrosin activation in the presence of a 32-kDa protein from boar spermatozoa. Biochem Biophys Res Commun 1989; 160:1026–1032.

Baba T, Niida Y, Michikawa Y, Kashiwabara S, Kodaira K, Takenaka M, Kohno N, Gerton GL, Arai Y. An acrosomal protein, sp32, in mammalian sperm is a binding protein specific for two proacrosins and an acrosin intermediate. J Biol Chem 1994a; 269:10133–10140.

Baba T, Azuma S, Kashiwabara S, Toyoda Y. Sperm from mice carrying a targeted mutation of the acrosin gene can penetrate the oocyte zona pellucida and effect fertilization. J Biol Chem 1994b; 269:31845–31849.

Bedford JM, Breed WG. Regulated storage and subsequent transformation of spermatozoa in the fallopian tubes of an Australian marsupial, Sminthopsis crassicaudata. Biol Reprod 1994; 50:845–854.

Buffone MG, Foster JA, Gerton GL. The role of the acrosomal matrix in fertilization. Int J Dev Biol 2008; 52:511–522.

Chang H, Suarez SS. Unexpected flagellar movement patterns and epithelial binding behavior of mouse sperm in the oviduct. Biol Reprod 2012; 86:1–8.

Coy P, García-Vázquez FA, Visconti PE, Avilés M. Roles of the oviduct in mammalian fertilization. Reproduction 2012; 144:649–660.

DeMott RP, Suarez SS. Hyperactivated sperm progress in the mouse oviduct. Biol Reprod 1992; 46:779–785.

Florman HM, Ducibella T. Fertilization in mammals. In: Neill JD (ed.), Knobil and Neill's Physiology of Reprodu ction. San Diego: Elsevier; 2006:55–112.

Fukuda N, Yomogida K, Okabe M, Touhara K. Functional characterization of a mouse testicular olfactory receptor and its role in chemosensing and in regulation of sperm motility. J Cell Sci 2004; 117:5835–5845.

Gaddum-Rosse P. Some observations on sperm transport through the uterotubal junction of the rat. Am J Anat 1981; 160:333–341.

Gillies E, Cannon R, Green R, Pacey A. Hydrodynamic propulsion of human sperm. J Fluid Mech 2009; 625:445–474.

Gomendio M, Malo AF, Garde J, Roldan ER. Sperm traits and male fertility in natural populations. Reproduction 2007; 134:19–29.

Hardy DM, Oda MN, Friend DS, Huang TT Jr. A mechanism for differential release of acrosomal enzymes during the acrosome reaction. Biochem J 1991; 275:759–766.

Hasuwa H, Muro Y, Ikawa M, Kato N, Tsujimoto Y, Okabe M. Transgenic mouse sperm that have green acrosome and red midpiece allow visualization of sperm and their acrosome reaction in vivo. Exp Anim 2010; 59:105–107.

Hino T, Muro Y, Tamura-Nakano M, Okabe M, Tateno H, Yanagimachi R. The behavior and acrosomal status of mouse spermatozoa in vitro, and within the oviduct during fertilization after natural mating. Biol Reprod 2016; 95:50.

Hirohashi N, Spina FAL, Romarowski A, Buffone MG. Redistribution of the intra-acrosomal EGFP before acrosomal exocytosis in mouse spermatozoa. Reproduction 2015; 149:657–663.

Ikawa M, Inoue N, Benham AM, Okabe M. Fertilization: a sperm's journey to and interaction with the oocyte. J Clin Invest 2010; 120:984–994.

Inoue N, Ikawa M, Isotani A, Okabe M. The immunoglobulin superfamily protein Izumo is required for sperm to fuse with eggs. Nature 2005; 434: 234–238.

Ishikawa Y, Usui T, Yamashita M, Kanemori Y, Baba T. Surfing and swimming of ejaculated sperm in the mouse oviduct. Biol Reprod 2016; 94:89.

Isotani A, Matsunuma T, Ogawa M, Tanaka T, Yamagata K, Ikawa M,

Okabe, M. A delayed sperm penetration of cumulus layers by disruption of acrosin gene in rats. Biol Reprod 2017; 97:61–68.

Kanemori Y, Ryu JH, Sudo M., Niida-Araida Y, Kodaira K, Takenaka M, Kohno N, Sugiura S, Kashiwabara S, Baba T. Two functional forms of ACRBP/sp32 are produced by pre-mRNA alternative splicing in the mouse. Biol Reprod 2013; 88:105.

Kanemori Y, Koga Y, Sudo M, Kang W, Kashiwabara S, Ikawa M, Hasuwa H, Nagashima K, Ishikawa Y, Ogonuki N, Ogura A, Baba T. Biogenesis of sperm acrosome is regulated by pre-mRNA alternative splicing of Acrbp in the mouse. Proc Natl Acad Sci U S A 2016; 113:3696–3705.

Kawano N, Kang W, Yamashita M, Koga Y, Yamazaki T, Hata T, Miyado K, Baba T. Mice lacking two sperm serine proteases, ACR and PRSS21, are subfertile, but the mutant sperm are infertile in vitro. Biol Reprod 2010; 83:359–369.

Kim KS, Gerton GL. Differential release of soluble and matrix components: Evidence for intermediate states of secretion during spontaneous acrosomal exocytosis in mouse sperm. Dev Biol 2003; 264:141–152.

Kimura M, Kim E, Kang W, Yamashita M, Saigo M, Yamazaki T, Nakanishi T, Kashiwabara S, Baba T. Functional roles of sperm hyaluronidases, HYAL5 and SPAM1, in fertilization in mice. Biol

Reprod 2009; 81:939–947.

Krzanowska H. The passage of abnormal spermatozoa through the uterotubal junction of the mouse. J Reprod Fertil 1974; 38:81–90.

Lishko PV, Botchkina IL, Kirichok Y. Progesterone activates the principal Ca^{2+} channel of human sperm. Nature 2011; 471:387–391.

Miyata H, Satouh Y, Mashiko D, Muto M, Nozawa K, Shiba K, Fujihara Y, Isotani A, Inaba K, Ikawa M. Sperm calcineurin inhibition prevents mouse fertility with implications for male contraceptive. Science 2015; 350:442–445.

Mizushima N, Yamamoto A, Matsui M, Yoshimori T, Ohsumi Y. In vivo analysis of autophagy in response to nutrient starvation using transgenic mice expressing a fluorescent autophagosome marker. Mol Biol Cell 2004; 15:1101–1111.

Mortimer ST. A critical review of the physiological importance and analysis of sperm movement in mammals. Hum Reprod Update 1997; 3:403–439.

Muro Y, Hasuwa H, Isotani A, Miyata H, Yamagata K, Ikawa M, Yanagimachi R, Okabe M. Behavior of mouse spermatozoa in the female reproductive tract from soon after mating to the beginning of fertilization. Biol Reprod 2016; 94:80.

Overstreet JW, Cooper GW. Effect of ovulation and sperm motility on the migration of rabbit spermatozoa to the site of fertilization. J Reprod Fertil 1979; 55:53–59.

Satouh Y, Inoue N, Ikawa M, Okabe M. Visualization of the moment of mouse sperm-egg fusion and dynamic localization of IZUMO1. J Cell Sci 2012; 125:4985–4990.

Shalgi R, Smith TT, Yanagimachi R. A quantitative comparison of the passage of capacitated and uncapacitated hamster spermatozoa through the uterotubal junction. Biol Reprod 1992; 46:419–424.

Smith TT, Koyanagi F, Yanagimachi R. Quantitative comparison of the passage of homologous and heterologous spermatozoa through the uterotubal junction of the golden hamster. Gamete Res 1988; 19:227–234.

Spehr M, Gisselmann G, Poplawski A, Riffell JA, Wetzel CH, Zimmer RK, Hatt H. Identification of a testicular odorant receptor mediating human sperm chemotaxis. Science 2003; 299:2054–2058.

Spina FAL, Molina LCP, Romarowski A, Vitale AM, Falzone TL, Krapf D, Hirohashi N, Buffone MG. Mouse sperm begin to undergo acrosomal exocytosis in the upper isthmus of the oviduct. Dev Biol 2016; 411:172–182.

Strunker T, Goodwin N, Brenker C, Kashikar ND, Weyand I, Seifert R,

Kaupp UB. The CatSper channel mediates progesterone-induced Ca^{2+} influx in human sperm. Nature 2011; 471:382–386.

Suarez SS, Pacey AA. Sperm transport in the female reproductive tract. Hum Reprod 2006; 12:23–37.

Suarez SS. Regulation of sperm storage and movement in the mammalian oviduct. Int J Dev Biol 2008; 52:455–462.

Toyoda Y, Yokoyama M, Hoshi T. Studies on fertilization of mouse eggs in vitro. Jpn J Anim Reprod 1971; 16:147–151.

Wang S, Larina IV. In vivo three-dimensional tracking of sperm behaviors in the mouse oviduct. Development 2018; 145:DOI 10.1242/dev.157685

Wilson-Leedy JG, Ingermann RL. Development of a novel CASA system based on open source software for characterization of zebrafish sperm motility parameters. Theriogenology 2007; 67:661–672.

Yamagata K, Murayama K, Okabe M, Toshimori K, Nakanishi T, Kashiwabara S, Baba T. Acrosin accelerates the dispersal of sperm acrosomal proteins during acrosome reaction. J Biol Chem 1998; 273:10470–10474.

Yamaguchi R, Yamagata K, Ikawa M, Moss SB, Okabe M. Aberrant distribution of ADAM3 in sperm from both angiotensin-converting

enzyme (Ace)- and calmegin (Clgn)-deficient mice. Biol Reprod 2006; 75:760–766.

Yamaguchi R, Muro Y, Isotani A, Tokuhiro K, Takumi K, Adham I, Ikawa M, Okabe M. Disruption of ADAM3 impairs the migration of sperm into oviduct in mouse. Biol Reprod 2009; 81:142–146.

Yamashita M, Honda A, Ogura A, Kashiwabara S, Fukami K, Baba T. Reduced fertility of mouse epididymal sperm lacking Prss21/Tesp5 is rescued by sperm exposure to uterine microenvironment. Genes Cells 2008; 13:1001–1013.

Yamazaki T, Yamagata K, Baba T. Time-lapse and retrospective analysis of DNA methylation in mouse preimplantation embryos by live cell imaging. Dev Biol 2007; 304:409–419.

Yanagimachi R. Mammalian fertilization. In: Kobil E, Neill JD (eds.), The Physiology of Reproduction, vol. 1. New York: Raven Press; 1994:189–317.

Yoshida M, Murata M, Inaba K, Morisawa M. A chemoattractant for ascidian spermatozoa is a sulfated steroid. Proc Natl Acad Sci U S A 2002; 99:14831–14836.

Zhou C, Kang W, Baba T. Functional characterization of double-knockout mouse sperm lacking SPAM1 and ACR or SPAM1 and PRSS21 in fertilization. J Reprod Dev 2012; 58:330–337.

Finally, I would like to give my special thanks to my parents Hiroshi and Mikiko, to my brothers Tooru and Takashi, and to my wife Rieko.